IOP Conf. Series: Materials Science and Engineering **361** (2018) 012012 doi:10.1088/1757-899X/361/1/012012

Vibration suppression with electromagnetic hybrid vibration isolators

Fan Chen

School of Mechanical Science and Engineering, Huazhong University of Science and Technology, Wuhan, China

Email: chenf04@163.com

Abstract. The design and control of a novel electromagnetic hybrid vibration isolator is presented in this paper. In the proposed hybrid vibration isolator configuration, an electromagnetic actuator and a rubber vibration isolator are configured in a parallel structure with the rubber vibration isolator installed inside the mover of the actuator. The magnetic force of the actuator is linearized by magnetic configuration design. Filtered-x least mean square (FxLMS) control algorithm is implemented for hybrid vibration isolation. Experimental results show that the vibration is suppressed significantly with the proposed hybrid vibration isolator and the FxLMS control algorithm.

1. Introduction

Large rotary machines, like diesel engines and large motors, always cause severe vibration problems and induce a lot of noise. Passive rubber vibration isolators[1], are normally used for vibration isolation of these kinds of large rotary equipments. However, for low frequency vibration isolation, the performance of passive isolators are quite limited. Hybrid vibration isolators combine passive isolators and actuators together, and use active control laws to suppress the vibrations. Comparing to passive isolators, the hybrid vibration isolator can not only damp the high frequency vibrations, but also obtain better performance in the low frequency region. In a hybrid vibration isolator, the passive isolator and the actuator can be structured either in series or in parallel.

For hybrid vibration isolators structured in series, Chen and Shih[2] presented a hybrid pneumatic vibration isolator, in which an active pneumatic actuator and a passive pneumatic vibration isolator were connected in series. The passive pneumatic isolator was used to support the gravity of the payload, while the active pneumatic actuator was used to suppress the low frequency disturbances. However, the size of the proposed hybrid vibration isolator is too large to be implemented. Gao et al.[3] proposed a compact hybrid vibration isolator structure, in which a piezoelectric actuator and a passive rubber vibration isolator were integrated in series. They reported a 10dB reduction in the vibration transmissibility over the purely passive ways. But for piezoelectric actuators, the stroke is only several dozens of micrometers, thus restricting the vibration isolation performance[4].

For hybrid vibration isolators configured in parallel, Liu[5] built a hybrid vibration isolation system in which a voice coil actuator worked in parallel with four springs. Ahn et al.[6] installed an electromagnetic actuator in parallel with three pneumatic vibration isolators, and built a hybrid vibration isolation system. The work in [5] and [6] demonstrated that the parallel structured hybrid vibration isolation system can achieve a good vibration isolation performance. But the proposed

configurations take up too much space. To be more practical for implementation, the actuators and the passive vibration isolators need to be integrated more compactly as one vibration isolator. Daley et al.[7] presented a compactly designed hybrid vibration isolator in which an electromagnetic actuator and several springs are structured in parallel. Li et al.[8] proposed to integrate an electromagnetic actuator inside a pneumatic vibration isolator to develop a new type of compact hybrid vibration isolator. However, the electromagnetic actuators in [7, 8] have nonlinear force-current relations, which complex the controller design. Also, integrating the electromagnetic actuator inside the passive vibration isolator restricts the actuator size as well as the maximum magnetic force output, therefore, limits the achievable vibration isolation performance.

This paper presents a novel parallel configured electromagnetic hybrid vibration isolator, in which the electromagnetic actuator is designed to have a linear relationship between the magnetic force and the coil current, which can simplify the controller design process. In the proposed hybrid vibration isolator structure, a passive rubber vibration isolator is installed inside the electromagnetic actuator. Therefore, the actuator size is not limited by the passive isolator, and can be designed to generate larger magnetic force which allows the hybrid vibration isolator to achieve a better performance. FxLMS control algorithm is implemented for hybrid vibration isolation. Experimental results show that significant vibration reduction is achieved with the proposed hybrid vibration isolators and the FxLMS control algorithm.

2. Electromagnetic hybrid vibration isolator design

2.1. Configuration of the hybrid vibration isolator

The configuration of the proposed hybrid vibration isolator is shown in Figure 1 (a) and the fabricated prototype hybrid vibration isolator is shown in Figure 1 (b). The designed hybrid vibration isolator is mainly composed of a rubber vibration isolator, an electromagnetic actuator, a base, a safety plate and a connector. The electromagnetic actuator includes a moving part and a stationary part. The mover of the actuator comprises armature cores and permanent magnets. The stator of the actuator includes stator cores and a coil which are boned together with epoxy. The electromagnetic actuator and the rubber vibration isolator are connected in parallel, and the rubber vibration isolator is installed inside the mover of the actuator. The stator of the actuator is fixed to the base. The connecter is used for installing the hybrid vibration isolator underneath the vibrating structure. The aluminum safety plate and the rubber pad are used to protect the mover of the actuator from collision during the vibration isolation process. An accelerometer is glued to the base of the hybrid vibration isolator to measure the acceleration signals of the base for real time control.

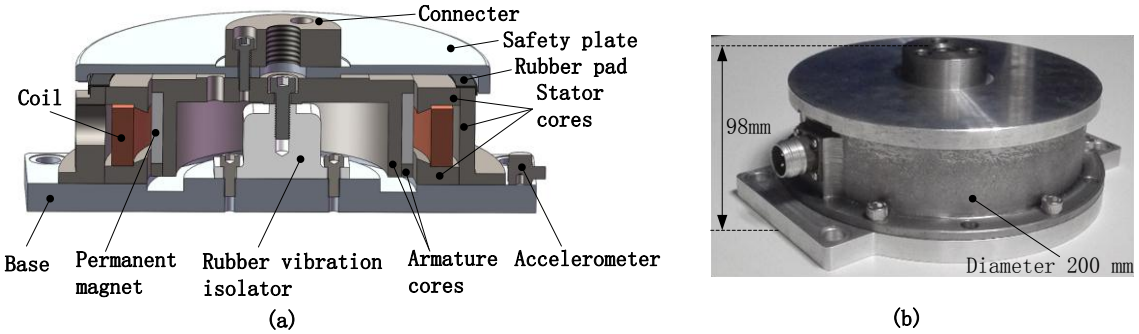

Figure 1. Configuration of the hybrid vibration isolator, (a) 3D model; (b) Fabricated prototype.

2.2. Working principle of the electromagnetic actuator

The magnetic configuration of the proposed electromagnetic actuator is shown in Figure 2. The coil and the stator cores work as an electromagnet when the coil is supplied with current. If the current direction in the coil and the magnetization direction of the permanent magnet are the same as the ones

shown in Figure 2, the directions of the magnetic flux flowing through the stator cores will be clockwise. Then, a north pole and a south pole will be generated at the lower and upper sides of the stator, respectively. The mover of the actuator will sense a repelling force at the lower air gap and an attractive force at the upper air gap. Thus, a net force in the positive y direction will be generated on the mover. If the current direction reverses, the force direction will change accordingly.

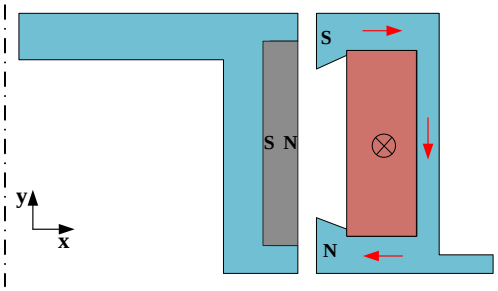

Figure 2. Magnetic configuration.

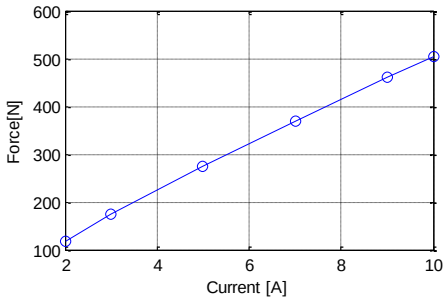

Figure 3. Force-current relation.

Denote the magnetic flux flowing through the air gaps between the upper magnetic poles, and between the lower magnetic poles as Φ1, Φ2 respectively. Then, for the magnetic configuration shown in Figure 2, we have:

$$\begin{aligned} \Phi_1 &= B_1 A = \bar{\Phi}_1 - \tilde{\Phi} \\ \Phi_2 &= B_2 A = \bar{\Phi}_2 + \tilde{\Phi} \end{aligned} \tag{1}$$

where B_1 and B_2 are the magnetic flux densities in the upper and lower air gaps, A is the area of the magnetic poles. $\bar{\Phi}_1$ and $\bar{\Phi}_2$ are the biasing flux generated by the permanent magnets, and $\tilde{\Phi}$ is the excitation flux generated by the coil.

According to [9], when the mover has very small displacements Δy from the central position, the variation of flux linkage is obtained as:

$$\begin{aligned} \Delta\psi &= N(\Delta\Phi_1 + \Delta\Phi_2) \\ &= 2NB_m d_g \, \Delta y \end{aligned} \tag{2}$$

and the thrust force can be calculated as:

$$F = I\frac{\Delta\psi}{\Delta y} = 2NB_m d_g \cdot I = K_i \cdot I \tag{3}$$

where N is the number of coil turns, B_m is the biasing flux density in the air gaps generated by the permanent magnet, d_g is the central diameter of the air gap, K_i is the magnetic force coefficient, and I is the amplitude of the coil current. It can be seen that the thrust force F generated by the electromagnetic actuator is proportional to the amplitude of the coil current I. The experimentally measured force -current relation is shown in Figure 3, which verifies the linearity of the actuator.

3. Experimental setup

In order to test the performance of the proposed novel hybrid vibration isolators, an experimental setup is built as shown in Figure 4. A shaker is used as the vibration source to simulate the vibration effects of rotary machines. Four hybrid vibration isolators are installed between the top and base steel plates at the four corners. Four BE85 rubber vibration isolators are installed underneath the base plate to support the whole experimental setup. An accelerometer is installed nearby the shaker to measure the reference vibration signals. The embedded accelerometers within the hybrid vibration isolators are used to measure the vibrations transmitted to the base. A multichannel signal conditioner is used to power the ICP accelerometers and transfer the acceleration signals to the dSPACE control system for active vibration suppression. Control algorithm is developed in a desktop computer with Matlab software, and is downloaded into the dSPACE control system for real time vibration control. Power

amplifiers receive the command signals generated from the dSPACE control system, and power the shaker and hybrid vibration isolators.

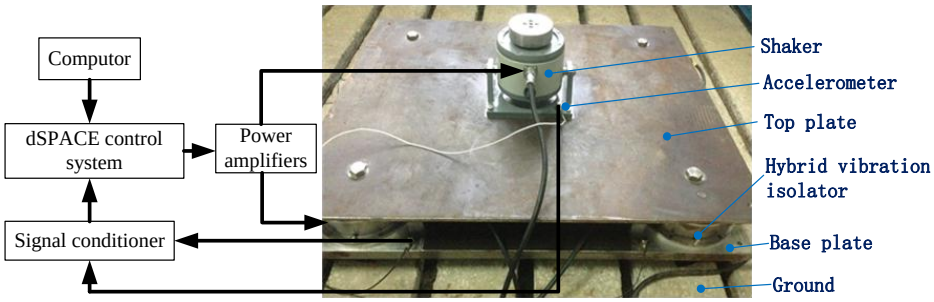

Figure 4. Experimental setup for hybrid vibration isolation tests.

4. Controller design

A single channel FxLMS control algorithm is developed in this work for prototype demonstration. Only the hybrid vibration isolator on the left-down corner of the experimental setup is controlled in this experiment. The block diagram of the control system is given in Figure 5. *P(z)* is the primary path dynamic response relation between the reference acceleration signal (*x(n)*) measured close to the shaker and the error acceleration signal (*d(n)*) measured nearby the hybrid vibration isolator. *S(z)* represents the secondary path frequency response function from the control signal (*y(n)*) to the error acceleration signal ($d_y(n)$) measured nearby the hybrid vibration isolator. The total error acceleration signal (*e(n)*) sensed by the accelerometer is $d(n)$-$d_y(n)$. The reference signal (*x(n)*) and error signal (*e(n)*) are passed to the FxLMS controller to calculate the control signal (*y(n)*).

In the FxLMS controller structure, a finite impulse response (FIR) filter (denoted as $\hat{S}(z)$) is used to model the secondary path (*S(z)*) of the control system, and the coefficients of the FIR filter ($\hat{S}(z)$) are identified offline using the least mean square (LMS) method. The estimated secondary path model ($\hat{S}(z)$) is used to filter the reference signal (*x(n)*). Another FIR filter (*W(z)*) is used as the controller, and its coefficients are updated in real time using LMS method based on the filtered reference signal (*r(n)*) and the error signal (*e(n)*). The controller coefficients and the control signal can be calculated with the following equations[10]:

$$\mathbf{w}(n+1) = \mathbf{w}(n) + \mu e(n)\boldsymbol{r}(n) \tag{4}$$

$$y(n) = \mathbf{w}(n)^{\mathrm{T}}\mathbf{x}(n) \tag{5}$$

where μ is the step size, $\mathbf{w}(n) = [\mathrm{w(n)\ w(n-1)\ ...\ w(n-M+1)}\ ]^{\mathrm{T}}$ is the controller coefficients vector, M is the tap length of the controller (*W(z)*), $\boldsymbol{r}(n) = [\mathrm{r(n)\ r(n-1)\ ...\ r(n-M+1)}\ ]^{\mathrm{T}}$, $\boldsymbol{x}(n) = [x(\mathrm{n})\ x(\mathrm{n}-1)\ ...\ x(\mathrm{n}-\mathrm{M}+1)\ ]^{\mathrm{T}}$.

5. Results analysis

During the vibration control experiments, the step size (μ) and tap length (M) of the controller (*W(z)*) are selected to be $\mu=10^{-5}$, M=500. A periodic disturbance which contains two different frequency components (55 Hz and 155 Hz) are generated with the shaker as the vibration source. The vibration level of the base plate at the hybrid vibration isolator location is measured and compared with and without control. When the controller is turned off, the base plate is vibrating severely, large peaks at 55 Hz and 155 Hz can be clearly seen from the frequency spectrums of the base plate vibration signals, as shown in Figure 6. When the controller is turned on, the acceleration amplitude of the base plate drops dramatically, the frequency spectrums of the base plate vibration signals at 55 Hz and 155 Hz are suppressed by 21.2dB and 27.9dB, respectively.

6. Conclusion

The design of a novel hybrid vibration isolator which contains a linear electromagnetic actuator and a rubber vibration isolator is presented in this paper. The actuator and the rubber

vibration isolator are configured in a parallel structure with the rubber vibration isolator installed inside the mover of the actuator. The magnetic force generated by the actuator has a linear relationship with the amplitude of the coil current which is verified through experimental measurements. An experimental setup is built with the proposed hybrid vibration isolators, and a FxLMS controller is developed for prototype demonstration. The experimental results show that the vibration level of the base plate and the acceleration transmissibility are decreased significantly with the proposed hybrid vibration isolator and the FxLMS control algorithm.

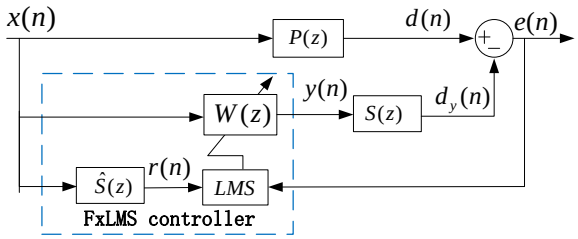

Figure 5. Block diagram of the control system using FxLMS algorithm.

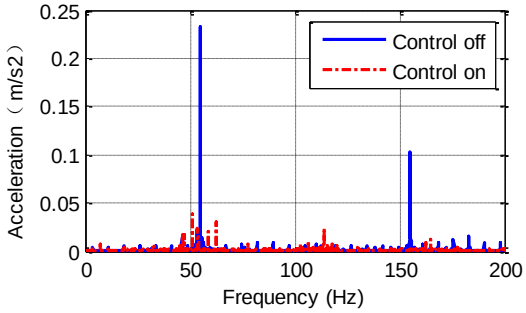

Figure 6. Frequency spectrums of the base plate vibration signals, with and without control.

References

[1] Chavan V S, Askhedkar R, and Sanap S B 2013 *Int. J. Eng. Res. Appl.* **3** 1423–28
[2] Chen P and Shih M, 2011 *J. Vib. Control* **17** 1325–36
[3] Gao J, Ji H and Qiu J 2015 *J. Vib. Shcock* **34** 141–8
[4] Chen P and Shih M 2007 *J. Vib. Control* **13** 1553–71
[5] Liu Y 2005 *J. Low Freq. Noise, Vib. Act. Control* **24** 181–90
[6] Ahn K G, Pahk H J, Jung M Y and Cho D W1996 *J. Sound Vib.* **192** 793–805
[7] Daley S, Johnson F A, Pearson J B and Dixon R 2004 *Control Eng. Pract.* **12** 465–74
[8] Li Y, He L, Shuai C and Lv Z 2014 *Tech. Acoust.* **33** 1–5
[9] Lu Q, Yu M, Ye Y, Fang Y and Zhu J 2011 *IEEE Trans. Magn.* **47** 4211–14
[10] Chang D and Chu F 2013 *IEEE Signal Process. Lett.* **20** 1122–25

Acknowledgement

This research was supported by the National Natural Science Foundation of China (Grant No. 51705175) and the China Postdoctoral Science Foundation (Grant No. 2017M612444).